GEOPHYSICAL RESEARCH LETTERS, VOL. 34, L06307, doi:10.1029/2006GL029106, 2007

Ocean bottom pressure changes lead to a decreasing length-of-day in a warming climate

Felix W. Landerer,[1] Johann H. Jungclaus,[1] and Jochem Marotzke[1]

Received 22 December 2006; revised 2 February 2007; accepted 26 February 2007; published 28 March 2007.

[1] We use a coupled climate model to evaluate ocean bottom pressure changes in the IPCC-A1B climate scenario. Ocean warming in the 21st and 22nd centuries causes secular oceanic bottom pressure anomalies. The essential feature is a net mass transfer onto shallow shelf areas from the deeper ocean areas, which exhibit negative bottom pressure anomalies. We develop a simple mass redistribution model that explains this mechanism. Regionally, however, distinct patterns of bottom pressure anomalies emerge due to spatially inhomogeneous warming and ocean circulation changes. Most prominently, the Arctic Ocean shelves experience an above-average bottom pressure increase. We find a net transfer of mass from the Southern to the Northern Hemisphere, and a net movement of mass closer towards Earth's axis of rotation. Thus, ocean warming and the ensuing mass redistribution change the length-of-day by −0.12 ms within 200 years, demonstrating that the oceans are capable of exciting nontidal length-of-day changes on decadal and longer timescales.
Citation: Landerer, F. W., J. H. Jungclaus, and J. Marotzke (2007), Ocean bottom pressure changes lead to a decreasing length-of-day in a warming climate, *Geophys. Res. Lett.*, *34*, L06307, doi:10.1029/2006GL029106.

1. Introduction

[2] Sea level changes can be attributed to changes of the total ocean mass (e.g., through the input of land water from glaciers), and to changes of the ocean density at constant ocean mass (steric changes). Steric changes occur through heating or cooling of the ocean; in a warming climate, the oceans take up most of the additional heat and hence thermosteric (temperature related) sea level rises significantly [*Gregory et al.*, 2001]. Steric changes do not alter the total global ocean mass, and are thus usually not associated with ocean bottom pressure (OBP) changes. However, heat uptake by the ocean varies locally, so a certain adjustment and redistribution of the mass of water can be expected. Specifically, it is interesting to consider how a thermosteric anomaly in the deep ocean transfers onto shallower shelf regions. *Ponte et al.* [2002] already pointed to a shift of mass from deep to shallow ocean areas in their study, but they did not analyze the pattern or processes in detail.

[3] Changes in ocean bottom pressure that are caused by ocean warming and circulation changes have not received much attention. The objective of our study is twofold: (1) We develop a simple conceptual model that relates ocean warming to secular bottom pressure changes, and we compare the simple model to the bottom pressure changes simulated in a coupled climate model. (2) We estimate the length-of-day changes (ΔLOD) associated with the change of Earth's moment of inertia through the simulated bottom pressure changes at constant global ocean mass.

2. Model and Methods

[4] We use the coupled Atmosphere-Ocean General Circulation-Model ECHAM5/MPI-OM from the Max Planck Institute of Meteorology in the setup that was used for the Intergovernmental Panel on Climate Change (IPCC) 4th assessment report. The general model behavior is discussed in detail by *Jungclaus et al.* [2006]. The horizontal resolution of the ocean/sea ice component MPI-OM varies between 12 km near Greenland and 180 km in the tropical Pacific; MPI-OM consists of 40 fixed vertical levels, 20 of which are distributed over the upper 700 m [*Marsland et al.*, 2003]. MPI-OM is coupled to the ECHAM5 atmosphere model at T63 horizontal resolution (corresponding to roughly 1.9°) with 31 vertical levels [*Roeckner et al.*, 2003]; no flux adjustments between the ocean and atmosphere model components are applied. Following the IPCC-A1B emission scenario [*Intergovernmental Panel on Climate Change*, 2001], the atmospher ic CO_2 concentration rises from 367 ppmv in the year 2000 to 703 ppmv by the year 2100; in the 22nd century, the atmospheric CO_2 concentration is held constant at 703 ppmv. Relative to preindustrial conditions, global mean thermosteric sea level rises 0.26 m by the year 2100, and 0.56 m by the year 2199 under the prescribed forcing [*Landerer et al.*, 2007].

[5] In our calculation of bottom pressure we follow *Ponte* [1999]. Bottom pressure is approximated by integrating the hydrostatic relation from the bottom $-H$ to the sea surface η, plus a spatially averaged barometric contribution $\bar{p_a}$, giving

$$p_b = g\rho_0\eta + g\int_{-H}^{0}\rho\, dz + \bar{p_a}, \tag{1}$$

where ρ_0 is a reference density for ocean water (here ρ_0 = 1028 kg/m^3), g is the gravitational acceleration on Earth's surface. Rearranging terms, the bottom pressure anomaly in time (indicated by a prime) with respect to a mean or unperturbed state is given by

$$\frac{p_b'}{g\rho_0} = \eta' - \eta_s' + \frac{\bar{p_a'}}{g\rho_0}, \tag{2}$$

[1]Max Planck Institute for Meteorology, Hamburg, Germany.

0094-8276/07/2006GL029106$05.00

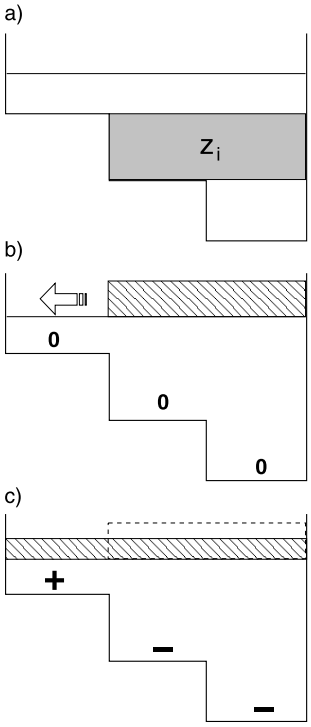

Figure 1. Simple redistribution model. (a) The shaded layer z_i is subject to a density anomaly ρ_i'. (b) The steric anomaly from layer z_i raises the sea surface locally. (c) The steric anomaly from layer z_i is spread over the entire ocean surface, leading to positive and negative bottom pressure changes as indicated (the steric anomaly is greatly exaggerated).

where η' is the anomalous sea surface height (SSH), and $\eta_s' = g\int_{-H}^{0}\rho'\,dz$ is the anomalous steric height. Note that the steric height deviation also includes local steric changes due to salinity anomalies, which can regionally be similar in magnitude to thermosteric signals, but often with opposite sign [*Landerer et al.*, 2007]. At periods longer than a few days, the ocean predominantly responds to atmospheric pressure anomalies isostatically like an inverted barometer (IB), so that p_a variations have no influence on the ocean dynamics [*Wunsch and Stammer*, 1997]. Consequently, the sea surface height term η in MPI-OM does not contain the IB effect. For present purposes, we set the mean atmospheric anomaly $\bar{p_a'}$ in equation (2) to zero, because we are interested in the pure oceanic signal. However, $\bar{p_a'}$ can vary in time and would have to be taken into account if one was interested in the atmospheric loading effect on ocean bottom pressure [*de Viron et al.*, 2002; *Ponte*, 1999].

[6] Furthermore, the formulation of the continuity equation in MPI-OM implies volume conservation rather than mass conservation. To ensure ocean mass conservation, we apply a time-varying but spatially uniform correction to the SSH to account for global mean sea level changes from global mean density changes [*Greatbatch*, 1994; *Ponte*, 1999]. In what follows, all anomalies are annual means and are taken relative to an unperturbed control climate (CO_2 concentration of 280 ppmv). We refer to bottom pressure changes in their normalized form ($p_b'/(g\rho_0)$, equation (2)), so that units are meters (of equivalent water column height).

3. Simple Redistribution Model

[7] Before we analyze the spatial pattern of bottom pressure changes in the IPCC-A1B scenario, we develop a simple conceptual model that explains to first order how a deep ocean warming can change bottom pressures at depths below and above the steric anomaly (Figure 1). In this approach, we assume that density changes occur uniformly in a certain depth layer, i.e. the density (and thus steric) anomalies are a function of depth only. The total ocean mass does not vary in time. To derive the model, it is sufficient to consider one layer at depth z_i with a height h_i and areal extent A_i, in an ocean with just three layers. Warming of this layer causes a negative density anomaly ρ_i' (Figure 1a), corresponding to a positive specific volume anomaly $\delta_i = \rho_i'/\rho_0$. Thus, the specific volume anomaly δ_i would raise the sea surface throughout the horizontal extent of layer i by $\delta_i h_i$, and lead to a sharp SSH gradient where the bathymetry becomes shallower (Figure 1b). With no forces present to balance this SSH gradient, we can assume that fast barotropic gravity waves immediately distribute the steric anomaly from layer z_i evenly across the entire ocean surface area A_s (Figure 1c). At this point, the deep warming and concurrent thermal expansion has led to a uniform global sea level rise, but mass redistribution within the basin has led to non-uniform bottom pressure changes. The gain in bottom pressure for the upper shallow layer is $\delta_i h_i$ (A_i/A_s), while the loss in bottom pressure for the layer z_i and each layer below is $\delta_i h_i[1 - (A_i/A_s)]$. Since mass is conserved, the sum of all bottom pressure changes is zero (e.g., in Figure 1, substitute $A_i/A_s = 2/3$, and sum up for all three layers). Generalizing this mechanism to n layers, and allowing for steric anomalies in all layers, we derive a discrete formulation for horizontally uniform, but vertically varying bottom pressure changes:

$$\frac{\Delta p_b(z_i)}{g\rho_0} = \sum_{i+1}^{n}\eta_s'(i) - \sum_{1}^{i}\left(\frac{A_s}{A_i} - 1\right)\eta_s'(i), \qquad (3)$$

where $i = 1, \ldots, n$ counts downward from the surface, and $\eta_s'(i) = (A_i/A_s)\ \delta_i h_i$ represents the steric sea level change contribution from layer i. Equation (3) states that a layer gains mass from the expansion of all layers below, and loses mass from its own expansion and expansion of all layers above. Equivalently, this statement also holds for negative expansion (contraction, or cooling), exchanging gains with losses and vice versa. Note, however, that steric expansion through warming is a very slow process compared to barotropic adjustment timescales in the real ocean. Therefore, the redistribution would always be immediate, and a SSH gradient as described in Figure 1b would not build up.

[8] In order to estimate the magnitude of bottom pressure anomalies from ocean warming as a function of depth and time in an ocean with realistic topography, we use equation (3) and apply it to the horizontally averaged steric changes in our IPCC-A1B scenario for each model layer (Figure 2). As the warming penetrates deeper into the ocean over time, positive bottom pressure anomalies develop above the warming, with highest amplitudes at the shallowest

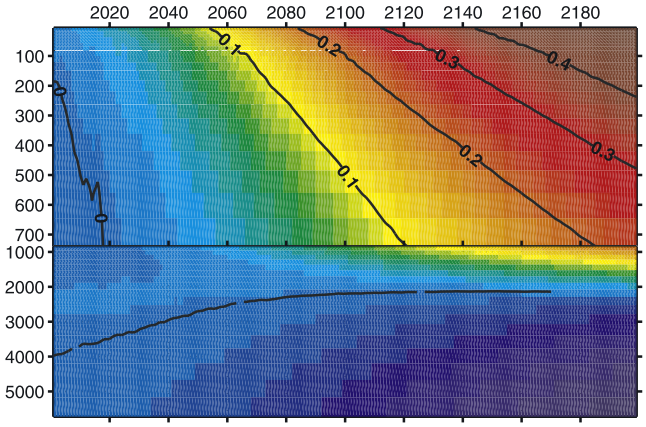

Figure 2. Bottom pressure changes with depth over time in the IPCC-A1B scenario as calculated from the simple redistribution model (equation (3)). Pressure is expressed in terms of equivalent water column height. Note split depth axis.

depths. The positive anomaly around 2500 m depth for the years 2001 to 2020 is due to a relative cooling (and thus negative steric anomaly) between 200 m and 1500 m depth, and might be linked to aerosol induced cooling carried over from the 20th century. After the year 2020, positive bottom pressure anomalies do not reach deeper than 2200 m, which approximately corresponds to the maximum depth where steric anomalies occur (with the exception of the Southern Ocean).

4. Spatial Pattern of p_b Anomalies

[9] Using equation (2), we have calculated the spatial pattern of bottom pressure anomalies for the time mean of the years 2090–2099 (Figure 3a). In many areas, bottom pressure anomalies correlate well with the ocean floor topography. While the deeper ocean areas show negative bottom pressure anomalies, larger positive anomalies up to 0.4 m appear in marginal seas and across shallow shelf areas. To examine how the simulated bottom pressure anomalies deviate locally from the simple redistribution model, we subtract the horizontally averaged $p_b(z_i)$ profile (time mean from 2090–2099 in Figure 2) from each simulated p_b anomaly in Figure 3a for corresponding bottom depths. This map reveals that regional bottom pressure anomalies can deviate by a similar order of magnitude from the global mean (Figure 3b). Especially the North Atlantic and Arctic Ocean shelves stand out: bottom pressure there increases substantially more than, for example, in the shelf areas of the Indonesian archipelago, where Δp_b is less than the global average. In the Indonesian archipelago, projected dynamic sea level changes are negative, consistent with the pattern of atmospheric circulation changes in the equatorial Pacific region (W. Müller and E. Roeckner, ENSO teleconnections in projection of future climate, submitted to *Climate Dynamics*, 2007).

[10] On a basin wide scale, the Atlantic and Pacific Oceans behave differently. Deep bottom pressure changes in the Atlantic have a larger amplitude than in the Pacific, which, together with the larger positive shelf signals in the Atlantic, is consistent with deeper reaching steric signals in the Atlantic Ocean as described by *Landerer et al.* [2007]. The pronounced negative anomaly in the Atlantic section of the Antarctic Circumpolar Current (ACC) can be associated with a spin up of the circulation through increased wind stress in the IPCC-A1B scenario [*Landerer et al.*, 2007]. By construction, the simple redistribution model cannot capture bottom pressure changes caused by circulation changes.

[11] A scatter plot of bottom pressure anomalies versus depth resolves basin wide and even regional variations (Figure 3c). For example, Baffin Bay and Labrador Sea bottom pressure changes (purple markers in Figure 3c) split into two branches below 650 m depth, which corresponds to the sill depth of Davis Straight. The deeper waters in Baffin Bay are isolated from the deep reaching steric anomaly

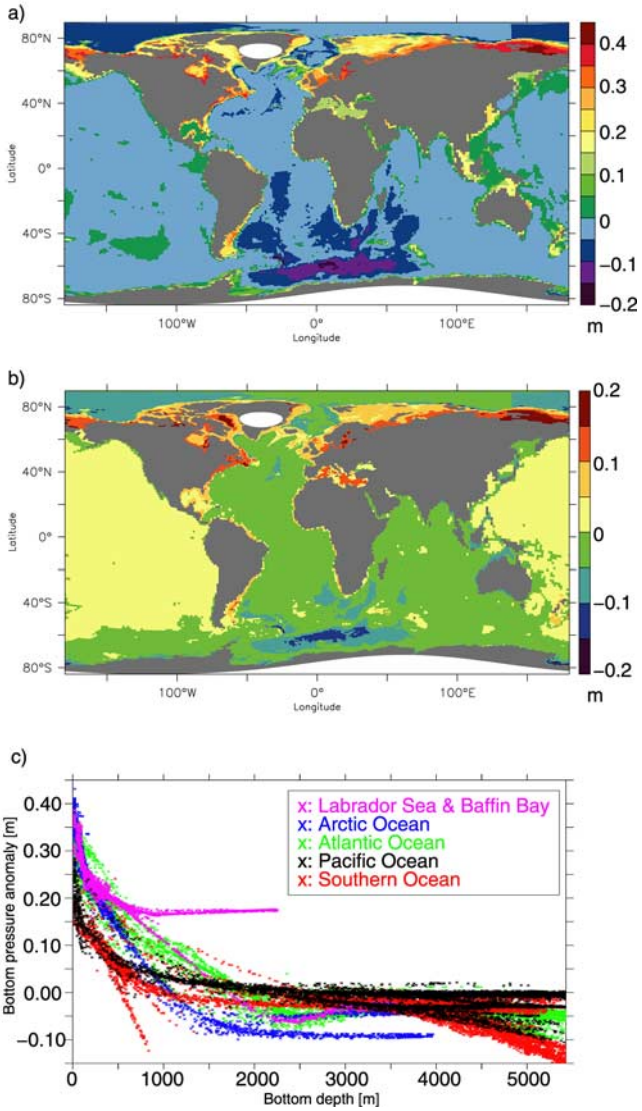

Figure 3. Bottom pressure anomalies for the years 2090–2099 (time mean). (a) Simulated bottom pressure changes. (b) Regional deviations: simulated anomalies minus 'simple redistribution' anomalies from Figure 2. (c) Simulated bottom pressure anomalies (from Figure 3a) versus topographic depth, color coded for different basins/regions. Pressure is expressed in terms of equivalent water column height.

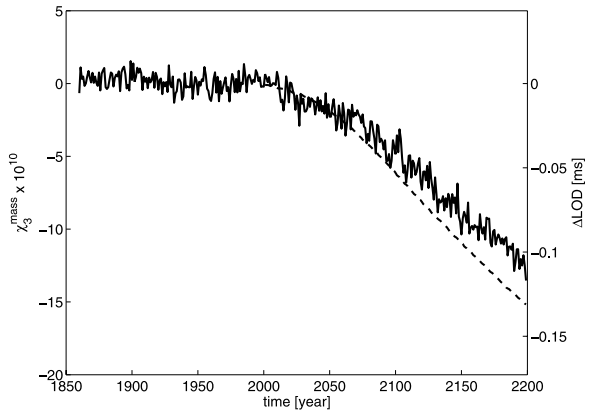

Figure 4. Oceanic Earth rotational excitation (left axis) and corresponding length-of-day changes (right axis) from the simulated pattern of bottom pressure anomalies (solid line), and from the simple redistribution model (dashed line).

signal that penetrates the central Labrador Sea through convection. In agreement with the horizontally averaged picture elucidated above (Figure 1), water would flow into Baffin Bay, increasing mass and hence bottom pressure there. A similar mechanism can explain the positive bottom pressure changes in the deep Gulf of Mexico and the Mediterranean.

5. ΔLOD from p_b Anomalies

[12] Bottom pressure anomalies are directly proportional to mass load anomalies, thus affecting Earth's gravity field and its moment of inertia [*Chao*, 1994; *Wahr et al.*, 1998]. Since the angular momentum (AM) of the total Earth system is conserved, Earth's rotation rate changes if its moment of inertia is altered via a redistribution of mass in the oceans. Note, however, that the atmosphere significantly influences the total AM budget under global warming on decadal and longer time scales [*de Viron et al.*, 2002].

[13] Following *Barnes et al.* [1983], we estimate the Earth rotational excitation χ_3^{mass} related to changes about Earth's polar axis from

$$\chi_3^{mass} = \frac{0.70 R_e^4}{I_{zz} g} \iint \Delta p_b(\theta, \lambda) \cos^3\theta \, d\theta \, d\lambda \qquad (4)$$

where R_e is the Earth's mean radius, I_{zz} is the principal moment of inertia, g is the gravitational acceleration, Δp_b are the bottom pressure anomalies described in sections 3 and 4, and θ and λ are latitude and longitude, respectively. The analysis reveals a clear secular trend in χ_3^{mass} (Figure 4), which corresponds to a length-of-day anomaly (ΔLOD) of nearly -0.12 ms by the year 2199 (for comparison, the motion term from ocean currents in the present simulation corresponds to $\Delta\text{LOD} \approx 0.026$ ms by 2199). The zonally integrated bottom pressure anomalies indicate a net transfer of mass from the Southern to the Northern Hemisphere (not shown). However, this mass transfer is not completely antisymmetric between the hemispheres, thus giving rise to a residual χ_3^{mass} anomaly. Essentially, mass is moved closer to the axis of rotation by means of redistribution within the ocean. To obtain a simple approximation to the χ_3^{mass} anomaly, we have re-calculated χ_3^{mass} with the horizontally averaged bottom pressure anomalies from the simple redistribution model (Figure 2), inserted into equation (4). Although the previous section showed that regional bottom pressure anomalies can deviate substantially from the horizontally averaged profile (Figure 3b), the simple redistribution model does capture a substantial part of the actual χ_3^{mass} signal (Figure 4, dashed line), but generally overestimates the amplitude by about 20%.

6. Concluding Discussion

[14] We have shown that ocean warming and circulation changes lead to significant secular bottom pressure changes in a warming climate. While the steric expansion does not change the total global ocean mass, mass is redistributed within and between ocean basins. An essential feature of our simulation is the strong positive bottom pressure anomaly on almost all shelf areas, while deep ocean regions show negative bottom pressure anomalies. Part of this mass redistribution can be explained by a simple redistribution model, which describes the bottom pressure anomalies as they should occur due to the decreasing ocean area with increasing depth, assuming in a first order approximation that steric anomalies from all depths are distributed evenly across the entire ocean surface. However, local bottom pressure anomalies can deviate by a similar order of magnitude from the global mean. This heterogeneous pattern reflects the differences in deep water formation in different ocean basins, thus affecting the penetration depth of the steric anomalies.

[15] Our simulated pattern of ocean bottom pressure anomalies leads to secular Earth rotational excitation of the axial component on relatively long time scales, corresponding to ΔLOD of nearly -0.12 ms after 200 years. Due to the somewhat fortuitous averaging out of longitudinal differences of bottom pressure anomalies between ocean basins (there is no dependence on longitude in the integration kernel in equation (4)), changes in χ_3^{mass} can be largely explained by the simple redistribution model. This finding implicitly links a global mean sea level rise to a reduction of LOD.

[16] In a slightly different warming scenario, *de Viron et al.* [2002] analyzed ΔLOD from an ensemble of coupled models. Under the assumption that the total mass term (atmosphere and ocean) is given only by the atmospheric mass term and the IB term over the ocean, they derive a mean ΔLOD trend of -0.75 μs/year for the mass term [*de Viron et al.*, 2002, Table 2]. However, as we show here, taking into account the term $\eta' - \eta_s'$ in equation (2) for the ocean mass term yields an additional trend of similar magnitude of -0.57 μs/yr. Ideally, this comparison should be done with the atmosphere mass term of the current generation IPCC-AR4 models, but this is beyond the scope of this paper. Our results are somewhat in contrast to *Ponte et al.*'s [2002], who did not detect significant LOD trends from ocean bottom pressure changes in a similar warming scenario simulation. We speculate that the discrepancy could be attributed to differences of the ocean warming patterns between the two simulations, and also to model

improvements in ECHAM5/MPI-OM over HadCM2, which was used by Ponte (R. Ponte, personal communication, 2006).

[17] On timescales of a few years and shorter, nontidal LOD variations are on the order of a few milliseconds, caused primarily by atmospheric angular momentum changes [*Gross et al.*, 2004]. Nontidal LOD variations on decadal and longer periods are primarily related to core-mantle interaction, with the atmosphere and oceans being relatively ineffective in exciting variations at these low frequencies [*Gross et al.*, 2004]. However, as we demonstrate here, ocean warming and the ensuing mass redistribution on these long time scales lead to a sizeable nontidal LOD anomaly. In principle, this anomaly is large enough to be measured and, in conjunction with observations of ocean thermal expansion, could help to constrain residuals (e.g., from core-mantle interaction) of future ΔLOD measurements.

[18] **Acknowledgments.** We thank E. Maier-Reimer for interesting discussions and the reviewers for helpful comments. This work was supported by the Max Planck Society and the International Max Planck Research School on Earth System Modelling. The computer simulations were performed at the DKRZ (Deutsches Klimarechenzentrum) in Hamburg, Germany.

References

Barnes, R. T. H., R. Hide, A. A. White, and C. A. Wilson (1983), Atmospheric angular momentum fluctuations, length-of-day changes and polar motion, *Proc. R. Soc. London, Ser. A*, *387*(1792), 31–73.

Chao, B. F. (1994), The geoid and Earth rotation, in *Geoid and Its Geophysical Interpretations*, edited by P. Vaníček and N. T. Christou, pp. 285–298, CRC Press, Boca Raton, Fla.

de Viron, O., V. Dehant, H. Goosse, M. Crucifix, and participating CMIP modeling groups (2002), Effect of global warming on the length-of-day, *Geophys. Res. Lett.*, *29*(7), 1146, doi:10.1029/2001GL013672.

Greatbatch, R. J. (1994), A note on the representation of steric sea level in models that conserve volume rather than mass, *J. Geophys. Res.*, *99*, 12,767–12,771.

Gregory, J. M., et al. (2001), Comparison of results from several AOGCMs for global and regional sea-level change 1900–2100, *Clim. Dyn.*, *18*, 225–240.

Gross, R. S., I. Fukumori, D. Menemenlis, and P. Gegout (2004), Atmospheric and oceanic excitation of length-of-day variations during 1980–2000, *J. Geophys. Res.*, *109*, B01406, doi:10.1029/2003JB002432.

Intergovernmental Panel on Climate Change, (2001), *Climate Change 2001: The Scientific Basis*, edited by J. T. Houghton et al., Cambridge Univ. Press, New York.

Jungclaus, J. H., N. Keenlyside, M. Botzet, H. Haak, J.-J. Luo, M. Latif, J. Marotzke, U. Mikolajewicz, and E. Roeckner (2006), Ocean circulation and tropical variability in the coupled model ECHAM5/MPI-OM, *J. Clim.*, *19*(16), 3952–3972.

Landerer, F. W., J. H. Jungclaus, and J. Marotzke (2007), Regional dynamic and steric sea level change in response to the IPCC-A1B scenario, *J. Phys. Oceanogr.*, *37*(2), 296–312.

Marsland, S. J., H. Haak, J. Jungclaus, M. Latif, and F. Röske (2003), The Max-Planck-Institute global ocean-sea ice model with orthogonal curvilinear coordinates, *Ocean Modell.*, *5*, 91–127.

Ponte, R. M. (1999), A preliminary model study of the large-scale seasonal cycle in bottom pressure over the global ocean, *J. Geophys. Res.*, *104*, 1289–1300.

Ponte, R. M., J. Rajamony, and J. M. Gregory (2002), Ocean angular momentum signals in a climate model and implications for Earth rotation, *Clim. Dyn.*, *19*, 181–190, doi:10.1007/s00382-001-0216-6.

Roeckner, E., et al. (2003), The atmospheric general circulation model ECHAM5, part I: Model description, *Tech. Rep. 349*, Max Planck Inst. for Meteorol., Hamburg, Germany.

Wahr, J., M. Molenaar, and F. Bryan (1998), Time variability of the Earth's gravity field: Hydrological and oeanic effects and their possible detection using GRACE, *J. Geophys. Res.*, *103*, 30,205–30,229.

Wunsch, C., and D. Stammer (1997), Atmospheric loading and the oceanic "inverted barometer" effect, *Rev. Geophys.*, *35*(1), 79–107.

J. H. Jungclaus, F. W. Landerer, and J. Marotzke, Max Planck Institute for Meteorology, Bundesstrasse 53, D-20146 Hamburg, Germany. (felix.landerer@zmaw.de)